JCTC Journal of Chemical Theory and Computation

pubs.acs.org/JCTC Article

# Conformational Sampling for Transition State Searches on a Computational Budget

Qiyuan Zhao, Hsuan-Hao Hsu, and Brett M. Savoie*

Cite This: https://doi.org/10.1021/acs.jctc.2c00081 Read Online

ACCESS | Metrics & More | Article Recommendations | Supporting Information

**ABSTRACT:** Transition state searches are the basis for computationally characterizing reaction mechanisms, making them a pivotal tool in myriad chemical applications. Nevertheless, common search algorithms are sensitive to reaction conformations, and the conformational spaces of even medium-sized reacting systems are too complex to explore with brute force. Here, we show that it is possible to train a classifier to learn the features of reaction conformers that conduce successful transition state searches, such that optimal conformers can be down-selected before incurring the cost of a high-level transition state search. The efficacy and transferability of this approach were tested using four distinct benchmarks comprising over three hundred individual reactions. Neglecting conformer contributions led to qualitatively incorrect activation energy estimations for a broad range of reactions, whereas simple random forest classifiers reliably down-selected low-barrier reaction conformers for unseen reactions. The robust performance of these machine learning classifiers mitigates cost as a factor when implementing conformational sampling into contemporary reaction prediction workflows and opens up many avenues for further improvements as transition state data grow.

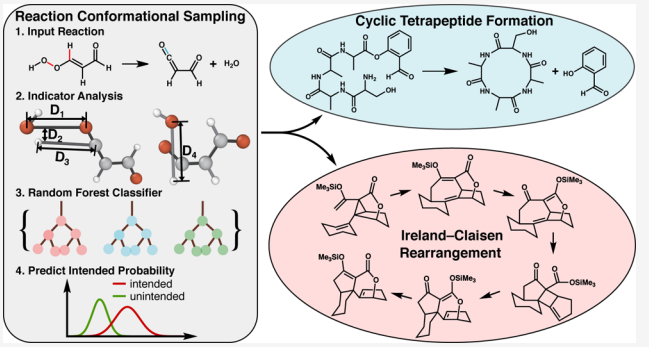




## 1. INTRODUCTION

Computational transition state (TS) characterizations are a standard tool for differentiating between competing reaction mechanisms and predicting reaction kinetics, making these calculations essential in manifold applications.[1−7] Nevertheless, searching for the TSs of large systems and complex reactions is still a fragile process that is heavily dependent on user expertise to guide search algorithms toward low-barrier crossings (e.g., by initializing the search geometry based on an anticipated mechanism). For this reason, recent method development efforts have been focused on automating the convergence of TS searches, thus eliminating potential biases from user interventions and democratizing the availability of these calculations.[4,5,7,8] One of the challenges to full automation is that the characteristics of discovered TSs, including the barrier height and identity of intermediates, can be profoundly affected by the conformational details of the reaction configuration. Although the significance of locating the most stable TS conformations has been widely discussed and some packages have been developed to achieve this goal,[9−11] there are currently no inexpensive means of automatically incorporating conformational sampling into TS characterization workflows, which limits its adoption in high-throughput and reaction discovery applications where conducting thousands of TS searches (or more) is routinely required.

Over the past several decades, many algorithms have been developed to localize the TSs of chemical reactions. Among the most efficient are so-called doubled-ended search (DES) algorithms that make use of reactant and product information to locate the TS. Two of the most commonly used DES algorithms are the nudged elastic band (NEB) and string methods. NEB methods pre-define the discrete points on the reaction path as images and optimize the images toward the minimum energy pathway (MEP),[12,13] while string methods, including the growing string method (GSM)[14,15] and the freezing string method (FSM),[16] add new images after each optimization step. All of these methods are pseudo one-dimensional searches to locate TSs under the geometric constraints of the reactants and products, which leads to a lower computational cost and wider application range compared with single-ended searching (SES) methods. In this sense, DES algorithms accelerate TS localization by using the mutual information of the starting (reactant) and ending points (products).

Despite the speedup enabled by DES algorithms, the details of a discovered TS are strongly impacted by the conformation

Received: January 23, 2022

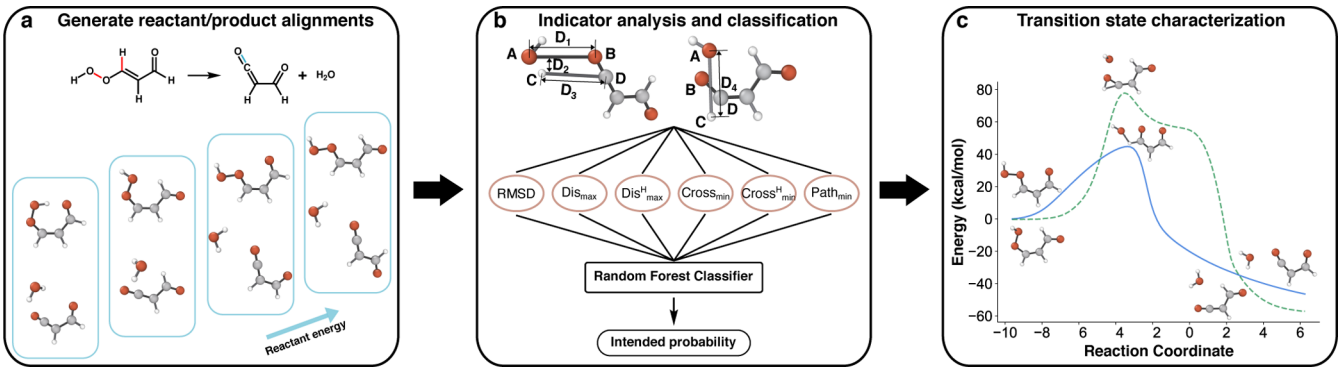


**Figure 1.** Overview of the presented approach for incorporating conformational sampling into an automated TS search. (a) Conformational sampling is performed on the reactants and/or products to yield M and N conformers, respectively. These conformers are then used to generate conformationally aligned reactant−product geometries (N + M, total) that are candidates for double-ended TS searches. (b) The RF classification model is employed to rank reactant−product geometries based on inexpensive geometric features. An example of one conformationally aligned reactant−product pair is shown. (c) TSs are characterized using growing string localization followed by Berny optimization and IRC calculations. An example is shown of a reaction with two qualitatively different TSs discovered from distinct reaction conformers.

that is used to set up the TS search. For example, misaligned reactant and product structures can stymie TS convergence.[15,17] Additionally, even when a TS converges, the barrier height and whether the TS corresponds to the intended reaction (i.e., a saddle point on the potential energy surface that corresponds to the putative reaction) strongly depend on the reaction conformation.[7] For a DES method, the possible conformational space of input structures is defined by the direct product of the reactant conformational space and the product conformational space. In this sense, $M$ reactant conformers and $N$ product conformers will lead to $M \times N$ possible conformational inputs to a DES method. Notably, the cost of sampling conformers for reasonably sized molecules is small (approximately quadratic in the number of atoms and with a small prefactor due to the semiempirical nature of available potentials) when compared with the computational cost of a TS search at chemically accurate levels of theory.[18,19] However, there is currently no means of down-selecting physically relevant conformers prior to performing a DES, which makes it common practice to neglect conformational sampling[4,20−22] or to only perform partial sampling of one or more discovered TSs.[19,23] The prospect of selecting optimal reaction conformers in advance is complicated by the fact that the energetically favored reactant and/or product conformer may not be germane to finding the lowest energy barrier of the intended reaction[24] (e.g., consider the relatively unfavorable cis diene conformation that is necessary for a Diels−Alder [DA] reaction). Thus, the cost of conformational sampling in a TS characterization workflow comes from the fact that putative reaction conformers must be subjected to expensive TS searches to determine their relevance and not from the conformer generation step itself.

The rationale for the current work is that if an indicator function could be developed that ranked conformers prior to performing a TS characterization, then the cost of incorporating conformational sampling into an automated DES workflow would be decimated. This strategy is motivated by the hypotheses that (i) although the conformational search space is formally $M \times N$, the number of reaction conformations leading to non-degenerate TSs is much smaller in practice, (ii) neglecting conformational sampling leads to errors that are consistently many times kT, and this confounds quantitative kinetic work, and (iii) since human intuition can often facilitate choosing a "good" conformer, the underlying fitness function is also amenable to being learned by a sufficiently flexible machine learning approach. Here, these hypotheses are interrogated by training the proposed indicator function and testing its performance on four reaction prediction benchmarks. These benchmarks are taken from several application areas and cover both simple and complex organic reactions, including $\gamma$-ketohydroperoxide decomposition, Ireland−Claisen rearrangement, competing DA reactions of a large ketothioester, and tetrapeptide cyclization. For all of these benchmarks, the trade-off between the completeness of conformational sampling and computational cost represents a major challenge for achieving automated and efficient localization of intended TSs. To perform these benchmarks, a modern conformational sampling algorithm was combined with our reaction prediction methodology, Yet Another Reaction Program (YARP),[7] to generate training data for developing and testing the transferability of the indicator function. The outcomes of these benchmarks demonstrate that conformational down-selection can be effectively performed across several reaction domains, thus representing a practical means of economically introducing conformational sampling into automated reaction prediction workflows.

## 2. METHODS

The reaction characterization performed in each benchmark consisted of three components: conformer generation, conformer classification, and TS characterization (Figure 1). Each component is described in the subsequent sections. In brief, conformational sampling of the reactant and product species was performed first, followed by the generation of conformationally aligned reactant−product pairs. After this step, inexpensive geometry-based indicators for each reactant−product alignment were calculated that served as input features for a random forest (RF)[25] classification model. Finally, the conformations were ranked by the RF model based on their probability of yielding an intended reaction channel and were then down-selected for TS characterization using YARP.

**2.1. Conformational Sampling of Reaction Geometries.** The conformers of both the reactant and product influence a double-ended TS search. Thus, the space of potential reaction conformers (i.e., the unique pairs of reactant and product conformers) is the product of these two


https://doi.org/10.1021/acs.jctc.2c00081
J. Chem. Theory Comput. XXXX, XXX, XXX−XXX

conformational spaces. Nevertheless, many such pairs are poorly conditioned for convergence since they may involve multiple dihedral rearrangements between reactants and products. Motivated by this, we recently developed an algorithm for generating conformationally aligned reactant−product pairs, based on the conformer of either one or the other.[7] For instance, given a conformer of the reactant (product), this algorithm generates a conformationally aligned product (reactant) geometry by performing a gradient descent optimization starting from the reactant (product) geometry but using a force-field potential and the bonding matrix of the product (reactant). Given the demonstrated robustness of this algorithm in earlier work, it is retained here for generating pairs of conformers after conformationally sampling the reactants or products. With this approach, the number of potential reaction conformations is reduced from $M \times N$ to $M + N$, where $M$ and $N$ are the number of conformers generated separately for the reactants and products, respectively.

Despite the reduction from $M \times N$ to $M + N$, there are still scenarios where conformational sampling is prohibitively costly with contemporary algorithms. For example, in an application like network exploration, there may be one set of reactants but hundreds of potential products. Likewise, many stereoisomers can result from the same set of reactants. In such cases, reactant-side conformational sampling can be several orders of magnitude less expensive than product-side sampling ($M \ll \Sigma_i N_i$, where $i$ indexes distinct products) due to the many candidate products. Additionally, constrained conformational sampling can be performed on already converged TSs to potentially discover more stable conformations.[8,19] Thus, conformational sampling of the reactant, product, and discovered TSs is all potentially relevant for finding the lowest barrier corresponding to the intended reaction. Unless stated otherwise, reactant-side conformational sampling is performed in the benchmarks reported here to keep the computational costs tractable, but in two of the benchmarks, the benefits of product-side sampling and TS conformational sampling are also compared.

All conformational sampling was performed using the CREST methodology,[19] which is a metadynamics-based algorithm for sampling the dihedral degrees of freedom (iMTD-GC algorithm) at the GFN2-xTB[26] level of theory. The thresholds for root-mean-squared displacement (RMSD) and energy used by CREST to determine distinct conformers were 0.125 Å and 0.05 kcal/mol, respectively. For multimolecular reactants, conformers were discarded if they exhibited a centroid−centroid intermolecular separation greater than twice the sum of the molecular radii. After conformational sampling and reactant−product alignment, an RMSD-minimized geometry was generated by rotation and center-of-mass translation to align the product with the reactant.[27] In our experience, RMSD minimization often helps, but it sometimes leads to geometries that fail to localize TSs compared with the merely conformationally aligned geometries. Here, whichever geometry exhibited a higher rank based on the RF model (vide infra) was retained, and the other was discarded.

**2.2. Ranking Reaction Conformations.** To rank reaction conformations, we developed a set of geometric features that would be inexpensive to calculate while also being sufficiently informative to train an accurate classifier. In particular, we anticipated that physically motivated features would enable us to train simpler ML models, like RFs, that can be applied with better transferability and reduced training data requirements than, say, a neural network.

In total, six geometric features were developed (Table 1). First, the mass-weighted root mean square displacement (RMSD) between the reactant and product geometries was computed to represent the overall structural change. Second, the maximum separation over all pairs of bonded atoms was defined to indicate the likelihood of fragment roaming. For this feature, a pair of atoms qualifies as bonded if a bond exists in either the reactant or in the product, not necessarily both. The separations of bonded pairs are calculated in both the reactant and product geometries, and the maximum over all of these separations comprises the feature. Because proton roaming is much more common and facile than other fragments' roaming (e.g., methyl and hydroxy), this feature was calculated separately with respect to bonded atoms involving hydrogen ($\mathrm{Dis}^{\mathrm{H}}_{\mathrm{max}}$) and bonded atoms only involving heavy atoms ($\mathrm{Dis}_{\mathrm{max}}$). For instance, $\mathrm{Dis}_{\mathrm{max}}$ of the reaction conformation shown in Figure 1b is the distance between oxygen atoms A and B in the product geometry (denoted as $D_1$ in Figure 1b), whereas $\mathrm{Dis}^{\mathrm{H}}_{\mathrm{max}}$ is taken from the larger value of the distance between the hydrogen atom, C, and the carbon atom, D, in the product geometry (denoted as $D_3$) and the distance between the oxygen atom, A, and the hydrogen atom, C, in the reactant geometry (denoted as $D_4$). To indicate the likelihood of a steric clash during the TS search, the minimum distance between segments connecting atoms forming bonds and segments connecting persistent bonds (i.e., unchanged bonds in the reaction) was calculated. If any atoms were shared between these two segments, then the combination was omitted since it would trivially yield zero. Similar to the previous case, $\mathrm{Cross}_{\mathrm{min}}$ and $\mathrm{Cross}^{\mathrm{H}}_{\mathrm{min}}$ were both calculated to distinguish between potential clashes involving only heavy atoms and those involving at least one hydrogen, respectively. An illustrative example of this feature is shown in Figure 1b where the distance between $D_4$ (i.e., the segment defining the eventual bond between hydrogen C and oxygen A) and the persistent bond between atoms B and D is close to zero. All else being equal, this is unfavorable since it implies that the atoms will have to bypass this chemical bond to complete the reaction. Finally, to indicate the likelihood of a steric clash between the reacting atoms (i.e., atoms involved in a bond that is broken or formed in a reaction), the minimum separations were calculated between the segments connecting each pair of heavy atoms that form a new bond during the reaction. The minimum separation over all such segments calculated in the reactant and product geometries comprises the feature $\mathrm{Path}_{\mathrm{min}}$.

**Table 1. Indicators for Selecting Reactant−Product Alignments**

| indicator | definition | threshold (Å) |
|---|---|---|
| RMSD | mass-weighted root mean square displacement | 1.8 |
| $\mathrm{Dis}_{\mathrm{max}}$ | maximum displacement over all bonded heavy atom pairs | 4.8 |
| $\mathrm{Dis}^{\mathrm{H}}_{\mathrm{max}}$ | maximum displacement over all bonded atom pairs involving at least one hydrogen | |
| $\mathrm{Cross}_{\mathrm{min}}$ | minimum separation between segments connecting bonded heavy atoms and persistent bonds | 0.03 |
| $\mathrm{Cross}^{\mathrm{H}}_{\mathrm{min}}$ | minimum separation between segments connecting bonded atoms involving hydrogen and persistent bonds | |
| $\mathrm{Path}_{\mathrm{min}}$ | distance between the reactive heavy atom segments | 0.20 |


https://doi.org/10.1021/acs.jctc.2c00081
J. Chem. Theory Comput. XXXX, XXX, XXX−XXX

Hydrogens were omitted from this feature since we found that clashes for protons are only weak indicators for a failure to localize a TS. For example, the distance $D_2$ shown in Figure 1b represents the minimum separation between the segments $D_1$ and $D_3$ which correspond to the bonds being formed during reaction. However, since bond segment $D_3$ involves a hydrogen, this separation is omitted from the calculation of $Path_{min}$. For any reactions where $Cross_{min}$ and $Path_{min}$ could not be calculated because all reacting bonds involved hydrogen, an above average value of 2.0 Å was used to indicate a low probability of a steric clash.

Before training or applying the RF model, reaction geometries were discarded if they exhibited features in excess of any of the thresholds listed in Table 1. These threshold values were chosen to be very conservative such that only very poorly conditioned geometries are excluded by these criteria (e.g., less than 1% of structures are discarded in this fashion). Examples of poorly conditioned geometries that fail these criteria are discussed in the Supporting Information (Figure S1).

Two RF models were trained that we will refer to as the "conformation-rich" and "conformation-poor" models. These models were trained on the same dataset, with the same indicators and hyper-parameters tuning the process, but they are distinguished by using true (intended) and false (unintended) class weight ratios of 1:1.5 and 1.5:1, respectively, during training. The reweighting of the class labels increases the penalty for false positives and false negatives in the conformation-rich and conformation-poor models, respectively. The rationale for this is that the two types of errors become problematic for different reasons in these data regimes and that both regimes can be encountered during conformational sampling. In the conformation-rich scenario, the surplus of conformers makes false positives a concern. In contrast, being too conservative in excluding false negatives can lead to too few conformers being sampled in the conformation-poor scenario. The model that was applied in each case was determined by the ratio of the total number of reaction conformations generated from the conformational sampling algorithm and the targeted number of conformations to be used for TS characterization ($N_{conf}$). Here, we used the conformation-rich model when this ratio was greater than 3; otherwise, the conformation-poor model was used. If the number of conformations classified as "intended" was greater than $N_{conf}$, all of these conformations were ranked by a scoring function—here, both the RF-predicted intended probability and the GFN2-xTB energy were considered as options—and the highest $N_{conf}$ conformations were selected; otherwise, all conformations that were classified as "intended" were retained for TS characterization.

Additional training details and the description of the training dataset can be found in Section S2 of the Supporting Information. In brief, the RF models were trained and tested on an 80:20 split of a dataset consisting of 1071 reactions (these geometries and pre-computed RF features are distributed as Supporting Information files). This dataset was drawn mainly from the original YARP publication and has no overlap with the reaction conformations used in any of the reported benchmarks. Thus, these benchmarks represent external testing evaluations of the transferability of these classifiers for down-selecting reaction conformers for TS searches.

**2.3. Characterizing TSs.** The performance of the reported classifier was measured by how well it predicted promising conformations for localizing intended TSs for reactions that were not used in training. YARP was used to localize and characterize the TSs of the benchmarked reactions.[7] These calculations consisted of performing a double-ended TS search using the GSM[15,28] at the GFN2-xTB level of theory, followed by DFT-level Berny optimizations to refine the TS and intrinsic reaction coordinate (IRC) calculations to characterize whether the resulting TS corresponded to the intended reaction. Once the TSs were characterized, activation energies were calculated with respect to the lowest-energy reactant conformer discovered during sampling (i.e., if two reaction conformations share a TS, then they will also exhibit the same activation energy). The number of DFT gradient calls performed during Berny optimization was used as a hardware-independent surrogate for the computational cost of each benchmark (Figure S9) since these calculations represent the most expensive step in the YARP calculation (>95%), with negligible computational costs associated with the geometry initialization and the GFN2-xTB gradient calls performed during the GSM calculations.[7] Several levels of DFT were used in this study since some of the benchmarks involved comparisons with previous studies. The corresponding functional and basis set is reported where each benchmark system is discussed.

Gaussian 16 was used as the reference quantum chemistry engine for the DFT calculations associated with the Berny optimizations and IRC characterizations.[29] The GSM calculations were performed by interfacing YARP with the pyGSM package[30] using most of the default convergence hyperparameters (e.g., the climbing image and the translation−rotation−internal coordinate system) with 9 nodes in the case of the relatively simple organic reaction benchmark and 11 nodes for all other cases. All GFN2-xTB calculations were performed with the xTB program (version 6.2.3) maintained by the Grimme group.[26] Universal Force Field (UFF)-based geometry optimizations were performed with Open Babel (version 2.4.1).[31] The Atomic Simulation Environment (ASE)[32] was called to apply the RMSD minimization. All simulations were run on a 448-node commodity cluster composed of two AMD Rome CPUs (2.0 GHz), 128 effective cores, and 256 GB of memory per node. DFT calculations were performed with 32-core parallelization, while all other calculations were performed as bundled single-core jobs.

## 3. RESULTS AND DISCUSSION

**3.1. Benchmark on Simple Organic Reaction Predictions.** The first benchmark was chosen to establish the impact of conformational sampling on relatively simple systems (e.g., less than 20 atoms).[33] For this purpose, we revisited 284 reactions from the original YARP study that failed to converge or localized to unintended TSs when characterized without conformational sampling. These reactions were generated by performing comprehensive graph-based reaction enumeration (i.e., all possible break-two bonds form two-bond reactions for each reactant) on 20 reactants from the Zimmerman dataset and γ-ketohydroperoxide.[7,34] Because these reactions are generated using graphical rules rather than established reaction templates, it is expected that many of them are intrinsically high-barrier or may not possess any intended TS even when a comprehensive search of the potential energy surface is possible. Among the 656 attempted reactions, YARP without


https://doi.org/10.1021/acs.jctc.2c00081
J. Chem. Theory Comput. XXXX, XXX, XXX−XXX

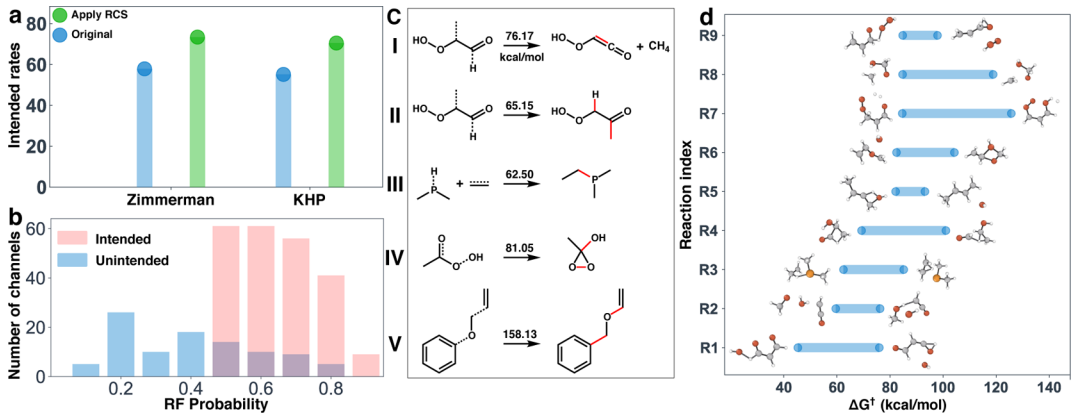


**Figure 2.** Overview of the performance of YARP with reaction conformational sampling on simple organic reactions. (a) Intended rate of reaction prediction for the Zimmerman and KHP datasets. The original results correspond to those reported in Ref. 7. (b) Distribution of RF-intended probabilities using the conformation-poor model applied to intended and unintended reaction conformations. (c) Five types of reactions where intended TSs were only discovered after conformational sampling. (I) E1 and E2 elimination reactions, appear 45 times out of 101 reactions, (II) small fragment-exchange reaction, appears 15 times, (III) addition and insertion reactions, appear 12 times, (IV) 3- and 4-membered ring closure reactions, appear 9 times, and (V) inner rotation reactions, appear 5 times. (d) Nine reactions with the range of activation energy distribution larger than 10 kcal/mol, the lowest- and highest-energy TS geometries are provided (gray: carbon, red: oxygen, yellow: phosphorus, white: hydrogen).

conformational sampling failed to converge at either the GSM, Berny optimization, or IRC calculation steps for 54 reactions and located unintended TSs for 230 reactions. Together, these 284 previously failed or unintended reactions were selected as a test for whether conformational sampling would yield intended TSs. Additionally, 35 reactions from the Zimmerman dataset that previously localized intended TSs were also included to ensure that the addition of conformational sampling did not inhibit localization of previously established TSs. Conformational sampling of all reactants was performed followed by down-selection of up to eight reaction conformers ($N_{conf}$ = 8). The reactions from the Zimmerman dataset and KHP systems were characterized at the B3LYP/6-31G** level to be consistent with earlier work.

For 270 out of the 284 previously failed or unintended reactions, reactant conformational sampling generated at least one conformation predicted by the RF model to yield an intended TS. For the remaining 14 reactions, no reaction conformation passed the indicator criteria, suggesting that these are fundamentally unphysical reactions (Figure S8). Among the 270 attempted reactions, YARP located at least one TS and one intended TS for 257 and 101 reactions, respectively, corresponding to a success and intended rate of 95.2 and 37.4%, respectively. Considering that 0% of this subset of reactions converged to an intended TS previously, this is a compelling demonstration that many reaction channels, even for small systems, can easily be neglected without conformational sampling. Out of the 35 previously intended reactions, all exhibited conformations that yielded intended TSs, demonstrating that the RF-based down-selection of conformers has no discernible negative impact compared with the previous algorithm. Accounting for the discovery of these intended TSs, the intended rate for the reactions in the Zimmerman dataset and KHP decomposition network is increased from 57.9 and 54.8 to 73.4 and 70.2%, respectively, compared with the earlier work (Figure 2a).

To illustrate the performance of the RF classifier, the predicted intended probabilities for unintended and intended reaction conformations from this benchmark are provided for the conformation-poor RF model (Figure 2b), which is biased against false negatives. The unintended conformers all come from the earlier study, whereas the intended conformers were those generated from conformational sampling and confirmed by IRC calculations. The intended conformers are all classified as such by the conformation-poor RF model (i.e., perfect recall), and the mean classification of the unintended conformers is unintended. This separation is favorable given the small number of features being used for the classification; nevertheless, a small number of unintended conformers still exhibit a high intended probability, which has motivated us to always choose $N_{conf}$ > 1 in all presented benchmarks. The corresponding RF predictions for the conformation-rich RF model are presented in Figure S6.

The 101 reactions that changed from unintended to intended were classified by mechanism (Figure 2c) to investigate why some of the reactions benefited from conformational sampling. By frequency, the five types of reactions are elimination (I, 45 out of 101 reactions), fragment exchanges (II, 15/101), addition and insertion (III, 12/101), 3- and 4-membered cyclizations (IV, 9/101), and inner rotations (V, 5/101), with the remainder composed of other mechanisms. I includes both E1 and E2 (i.e., unimolecular and bimolecular) eliminations; reaction II corresponds to the exchange in the position of two fragments, each consisting of no more than one heavy atom (e.g., in Figure 2c, a methyl group and a hydrogen atom exchange); and reaction V refers to a head-to-tail rotation of an internal segment of a reactant. Reactions I and II often occur as competing reactions involving the same bond breaks (i.e., they often localize an unintended TS that corresponds to the alternative). Notably, all of these mechanisms involve a large rotation or translation of atoms between their reactant and product geometries, such that conformational sampling is consequential despite the relatively small system size. Additional comparisons of intended and unintended TS geometries and for these classes of reactions are provided in Figure S7.

Conformational sampling also leads to the discovery of multiple TSs for many of the reactions that exhibit distinct mechanisms and a broad range of activation energies (Figure 2d). Out of 136 intended reactions (101 from previous unintended reactions and 35 from previous intended reactions), 9 exhibit multiple intended TSs with activation


https://doi.org/10.1021/acs.jctc.2c00081
J. Chem. Theory Comput. XXXX, XXX, XXX−XXX

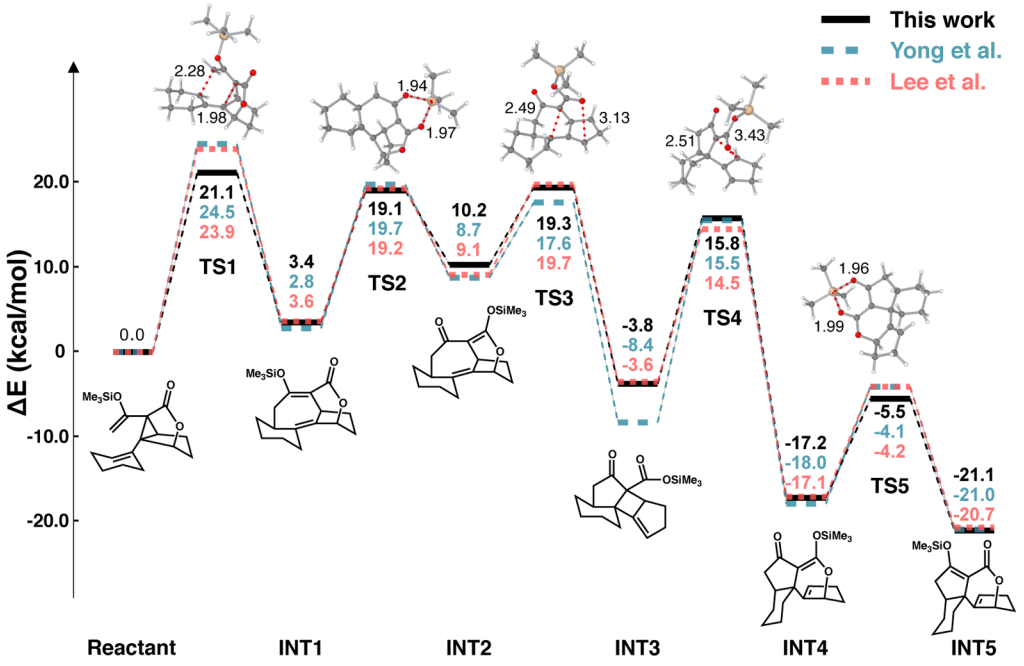


**Figure 3.** Ireland–Claisen rearrangement intermediate (INT) and TS energies calculated using YARP with conformational sampling (black) and energy profiles reported by Young et al.[8] (green) and by Lee et al.[35] (red). All curves are calculated at the B3LYP-D3BJ/6-311++G(2d,2p) and B3LYP-D3BJ/6-31G(d) levels of theory for the single-point calculations and geometry optimizations, respectively. The CPCM(hexane) solvent model was used in autodE, whereas the IEF-PCM(hexane) solvent model was used in this work and the work of Lee et al.

energies spanning more than 10 kcal/mol. These large differences in activation energies correspond to qualitatively different mechanisms in several cases. Considering reaction R1, for example, the higher-energy TS corresponds to the involvement of a hydrogen-roaming intermediate compared with the lower-activation energy pathway that bypasses roaming. In another example, reaction R7, the TS corresponding to a concerted reaction mechanism is much more stable than the TS corresponding to a sequential mechanism. Even in the cases where the range of activation energies for distinct TSs is less dramatic, the discovery of all low-lying TSs can be consequential for accurate kinetic modeling. In summary, even for this benchmark of reactions on small molecules, applying conformational sampling results in improved success rates, improved intended rates, and the discovery of lower-activation energy pathways.

**3.2. Ireland–Claisen Rearrangement.** The multi-step Ireland–Claisen rearrangement shown in Figure 3 was selected for the second benchmark since it exhibits increased conformational complexity and has recently been characterized using other automated TS localization methods. Lee et al.[35] proposed the illustrated Ireland–Claisen rearrangement pathway consisting of five sequential rearrangements as discovered by the combination of the trial-and-error and the artificial force-induced reaction (AFIR) method.[36] Young et al. performed a follow-up study using the autodE method and a heuristic for sampling conformations to localize distinct TSs.[8] Here, conformational sampling was performed on all five reactants to generate reaction conformers that were then ranked using the RF models to down-select up to eight reaction conformations for each step ($N_{conf}$ = 8). The TS localization was performed at the B3LYP-D3BJ/6-31G(d) level of theory and further evaluated at the B3LYP-D3BJ/6-311++G(2d,2p) level of theory with the IEF-PCM(hexane) solvent model to be consistent with the earlier study of Lee at al. Among the 40 total attempted reactions, all successfully localized a TS, and 37 were confirmed to be intended TSs after IRC characterization. In total, only 545 DFT gradient calls were used (13.6 per reaction) to locate these TSs. These two statistics indicate the high quality of the reaction conformations generated by RF ranking.

The three methods predict nearly identical single-point energies for the intermediates and TSs (Figure 3). The deviations among three methods are typically within 2 kcal/mol, indicating that similar reaction mechanisms are being described. Notably, YARP discovers a low-energy reaction conformation leading to a ∼3 kcal/mol reduction of **TS1**. Another large deviation of ∼5 kcal/mol is observed for **INT3** (i.e., not for a TS but for an intermediate). A more stable conformation is reported by Young et al., whereas the energies reported by Lee et al. and us are similar. This may be due to the distinct solvation model used by Young et al. in comparison with Lee et al. and the present work or differences in sampling the intermediate geometries. Nevertheless, the Ireland–Claisen rearrangement example demonstrates the transferability to more complex systems of the indicator function for down-selecting reaction conformations and the reproduction of TS energies achieved by contemporary approaches.

**3.3. Intramolecular DA Reactions of a Ketothioester.** For a third benchmark system, we investigated competing DA ring closures for the ketothioester shown in Figure 4. Although some cyclizations were present in the previous benchmarks, this case presents additional isomeric complexity, with 18 possible DA ring closures yielding up to 304 possible stereoisomers. In the context of a double-ended TS search, the product stereochemistry can be fixed by the user, but more generally, the relative likelihood of different product stereochemistries is something that a reaction prediction workflow would need to predict. With respect to conformational


https://doi.org/10.1021/acs.jctc.2c00081
J. Chem. Theory Comput. XXXX, XXX, XXX–XXX

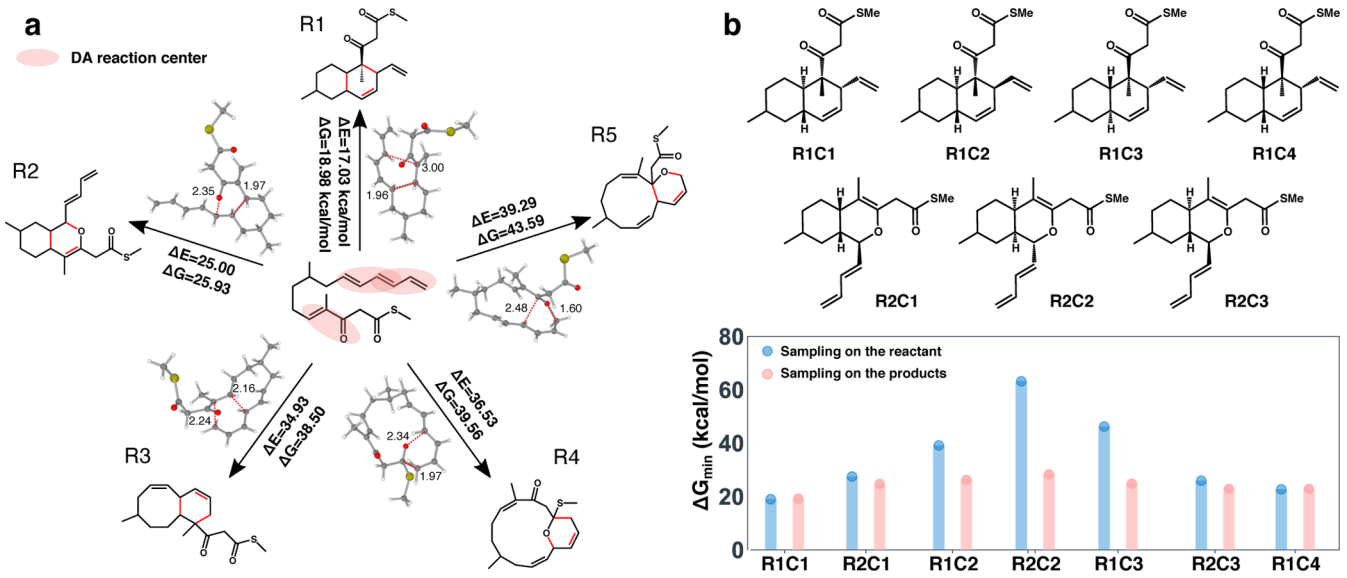


**Figure 4.** Five competing DA reactions of the ketothioester with activation energy lower than 40 kcal/mol. (a) Five DA products with corresponding activation energies ($\Delta E$), free energies of activation ($\Delta G$), and TS structures. The bonds denoted as red refer to bonds formed during the DA reaction. (b) Product conformations identified by YARP in the most favorable reaction 1 and 2. Corresponding free energies of activation are provided at the bottom.

sampling, this poses an additional challenge since reactant-side conformational sampling neglects the conformational constraints that are unique to each stereoisomer. However, performing product-side conformational sampling on all 304 distinct stereoisomers is wasteful since many, though not all, of the products can be ruled out using heuristics. To investigate this asymmetry, conformational sampling was first performed on the ketothioester reactant to generate 10 reaction conformations for each of the 18 possible DA reactions. These reaction conformations were ranked by the RF models; thus, the resulting stereoisomers were selected solely based on the likelihood that they would be connected by an intended TS rather than any chemical intuition. For a direct comparison with previous results, all TSs were optimized, and IRC calculations were performed at the B3LYP/6-31G level of theory (Figure S5). We also reperformed all single-point calculations at the more accurate B3LYP-D3BJ/def2-TZVP level of theory (Figure 4).

The reactant-side conformational search yielded at least one intended TS for all 18 attempted DA ring closures. Among them, five reactions exhibit activation energies less than 40 kcal/mol (Figure 4a). The two lowest-activation barrier reactions, denoted as R1 and R2, are two reactions reported previously by Yang et al.,[23] in an automated reaction prediction study focusing on a subset of reactive atoms of this ketothioester. In contrast, R3, R4, and R5 have not been previously reported. These reactions display larger barriers but are still potentially kinetically relevant. It is encouraging that YARP, with reactant-side conformational sampling, predicts the same lowest-barrier DA closures as in the earlier study despite not using a restricted subset of atoms.

The present benchmark found intended pathways to 38 distinct stereroisomers out of the 304 possible that could result from the 18 DA reactions. In the cases of R1 and R2, intended TSs were localized for 4 and 3 distinct enantiomers out of 32 and 16 possible, respectively. Six of these correspond to those previously reported by Yang et al.; R1C1 is new, and the earlier study reported intended TSs for two enantiomers that were not attempted here. Despite this large overlap in predicted enantiomers, several of the activation energies are overestimated using reactant-side conformational sampling (Figure 4b). In particular, we interpret this result as arising from the asymmetric conformational constraints of the reactant versus products in the case of these ring closures. To clarify this, we reperformed the TS searches for these seven enantiomers using product-side conformational sampling. In all cases, the activation energies discovered after product-side sampling are lower than those discovered from reactant-side sampling, and the differences in the activation energies for distinct enantiomers largely vanishe. This is a rather dramatic illustration of the inequivalence of reactant-side versus product-side conformational sampling. This asymmetry is present to varying degrees in any reaction, but it is acute for cyclizations and reactions yielding stereoisomers. In contrast, for the previous benchmarks, we observed relatively little distinction between performing conformational sampling on the reactants versus the products and then generating conformationally aligned structures.

**3.4. Head-To-Tail Cyclic Tetrapeptide Formation.** For a final benchmark, we selected the cyclic peptide formation of a series of large tetrapeptides. Peptide cyclization is challenging for TS searches because of the potentially large conformational search space of both the linear chains (reactants) and relatively large rings (products), in addition to the geometrically distinct bond-forming channels involving each amine hydrogen. Ring contractions are also relevant to these systems such that the conformational space of reactants and products is associated with distinct rings. For this benchmark, we selected a series of tetrapeptides that have been experimentally studied in the context of lowering the activation energy for accessing certain cyclic peptide products via tailored substitutions to the peptide backbone.[37] In particular, the SAAA tetrapeptide (Figure 5a) undergoes a relatively high-barrier cyclization via dehydration to form a 12-membered ring. SAAA-aux (Figure 5b) is hypothesized to undergo a facile ring contraction to the same 12-membered ring. Finally, SAAA-SAL (Figure 5c) was


https://doi.org/10.1021/acs.jctc.2c00081
J. Chem. Theory Comput. XXXX, XXX, XXX−XXX

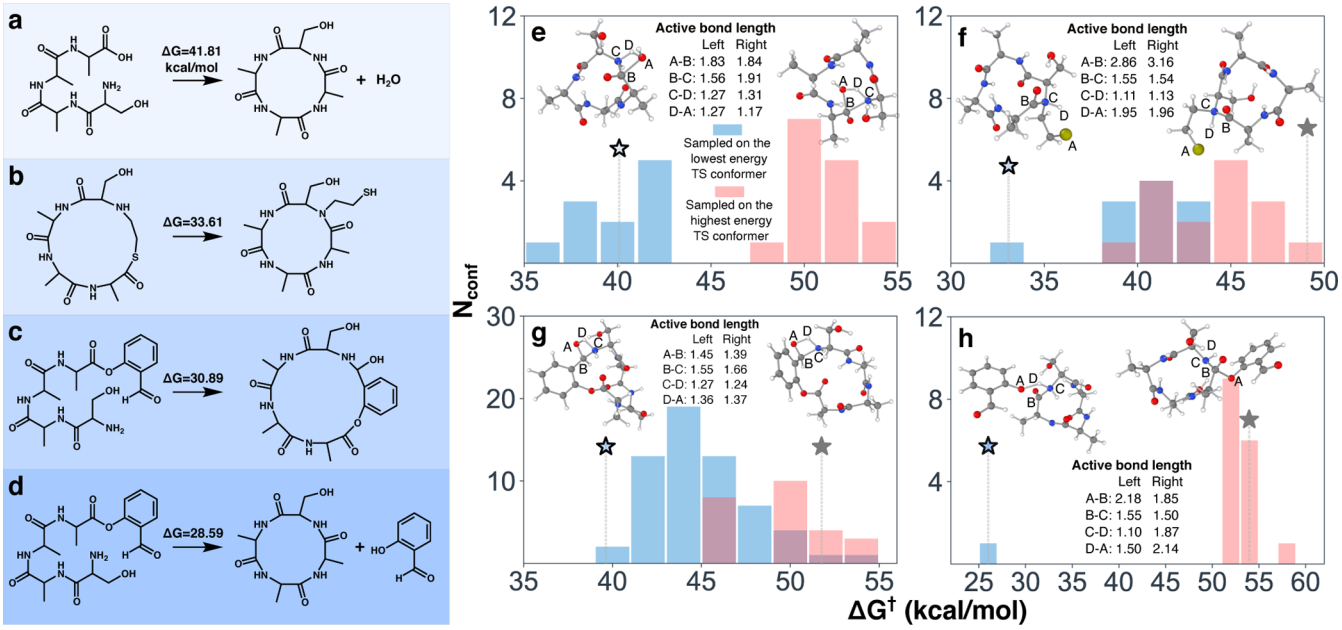


**Figure 5.** (a–d) Four cyclic tetrapeptide formation reactions with (a) D-seryl-D-alanyl-L-alanyl-D-alanine (denoted as SAAA), (b) 12-(hydroxymethyl)-3,6,9-trimethyl-1-thia-4,7,10,13-tetraazacyclopentadecane-2,5,8,11-tetraone (ethanethiol auxiliary SAAA, denoted as SAAA-aux), and (c,d) 2-formylphenyl D-seryl-D-alanyl-L-alanyl-D-alaninate (SAL-ester auxiliary SAAA, denoted as SAAA-SAL). The activation energies were computed at the M062X/6-311+G(d,p) level of theory on the geometries of the most stable TS sampled at the B3LYP/6-31G level. The SMD solvation model for acetic acid was applied. (e-h) Examples of TS conformational sampling starting from the lowest and highest TSs. The position of each star refers to the activation energy of the initial TS. The highest-energy TS in (e) is outside the axes. Constrained distances of all TSs are shown with unit Å. The lowest and highest free energies of activation ($\Delta G$) of (e-h) are 41.2/65.0; 32.5/49.5; 39.1/53.0; and 26.1/53.7 kcal/mol, respectively (computed at the B3LYP/6-31G level).

previously predicted to undergo cyclization to a 16-membered precursor that later undergoes more facile ring contraction to the 12-membered product, whereas the direct formation of the 12-membered product from SAAA-SAL (Figure 5d) was ruled out as being unfavorable. Some computational work has been done to rationalize these transformations,[37,38] but no DFT-level TSs have been calculated for these large and conformationally challenging systems.

Conformational sampling was performed on three different cyclic tetrapeptide precursors (Figure 5) to generate reaction conformers that were then ranked using the RF models to down-select up to 20 reaction conformations for each reaction ($N_{conf}$ = 20). YARP was first applied at the B3LYP/6-31G level to locate and characterize intended TSs. The most stable intended TSs for each reaction were further characterized at the M062X/6-311+G(d,p) level of theory (geometries taken from the B3LYP/6-31G results) with the SMD solvation model[39] for acetic acid, to match the level of earlier computational work.[37]

For all four reactions, the RF-ranked conformations converged to at least one intended TS (Figure 5a–d), which represents a first for all of these reactions. Based on the experimental data, it is expected that the introduction of the ethanethiol (Figure 5b) and SAL-ester (Figure 5c) auxiliaries will promote 12-membered cyclization in comparison with the SAAA cyclization (Figure 5a). The lowest-barrier-intended TS discovered for each reaction likewise confirms this trend. Interestingly, YARP predicts that the direct cyclization of the SAAA-SAL species is more favorable than proceeding through the 16-membered precursor that was previously invoked.[37]

Because these tetrapeptides are the largest systems investigated here, we decided to also use them as a case study of the potential benefits of performing conformational sampling on already localized TSs to search for a lower barrier crossing. In particular, several recent studies have used this approach,[8,19] but no direct comparison has been performed between TS conformational sampling and reactant-/product-side conformational sampling. Conformational sampling of TSs is more difficult than that of reactants or products, because a TS is a saddle point, and thus, conformational sampling can easily lead to an unintended reaction channel. To prevent this, auxiliary restraints are used for TS sampling that try to maintain the bond lengths of atoms involved in the imaginary frequency mode, but there is still no guarantee that the resulting TS conformer will remain an intended channel, and thus, it must be verified by further IRC calculations.

Constrained TS conformational sampling was applied to both the lowest- and highest-barrier-intended TSs obtained for the four tetrapeptide reactions. CREST was used to perform the TS conformational sampling while restraining the active bond (i.e., bonds broken or formed in each reaction) lengths to their distances in the corresponding intended TS (these distances are shown in the inset of Figure 5e–h). This procedure was based on that of the original CREST study;[19] however, the specific performance of TS conformational sampling may be strongly affected by the strength and types of auxiliary constraints used during sampling. The TS conformations generated in this way were then subjected to Berny optimization and IRC calculations, and the distribution of barrier heights for the intended TSs is reported in Figure 5e–h. TS conformational sampling on the lowest-barrier-intended TSs (stroked star marker) had only a marginal benefit. For three of the cases, all of the discovered TSs are of an equal or higher barrier compared to the original intended


https://doi.org/10.1021/acs.jctc.2c00081
J. Chem. Theory Comput. XXXX, XXX, XXX–XXX

TS. For SAAA, the majority of new TSs were also of an equal or higher barrier, but four lower-barrier TSs exhibiting up to a 5 kcal/mol reduction were discovered. In contrast, performing TS sampling on the highest-barrier-intended TSs from the original benchmark (filled star marker) yielded new lower-barrier TSs in all cases. Yet critically, none of these new TSs exhibit lower barriers than the lowest-barrier TS discovered from the original reactant-side conformational sampling search (i.e. the stroked star marker in Figure 5e−h).

Our interpretation of this case study on TS conformational sampling is that it can lead to barrier reduction in some cases, but it is strongly dependent on the TS used to seed the search, and it is not a substitute for reactant- and/or product-side conformational sampling. Moreover, computational cost and efficiency are important factors in deciding whether to use TS conformational sampling. On average, 26 conformers were generated by CREST for each of the 8 TSs used to seed the TS conformational search. This is more than $N_{conf}$ used for reactant-side sampling. Additionally, the intended rate of the generated TS conformers varies greatly between 100 and 3% (Figure S4). For these reasons, TS conformational sampling as currently implemented remains a costly procedure of marginal benefit.

## 4. CONCLUSIONS AND OUTLOOK

The maturation of conformational sampling algorithms has created new opportunities to incorporate conformational exploration into automated TS searches. Nevertheless, the cost of performing parallel TS searches starting from all possible reaction conformers remains prohibitive for applications, such as reaction network exploration, where performing hundreds to thousands of TS searches is typical. Here, we have shown how this limitation can be sidestepped using a relatively simple RF classifier to rank reaction conformations before performing costly TS searches. The performance of this approach was investigated in four distinct benchmarks. First, we demonstrated that intended TSs could be localized for over a hundred reactions (~39% of those attempted) that could not be converged using earlier algorithms. Likewise, conformational sampling revealed many competing barriers for these reactions that would have been otherwise missed. Second, in head-to-head comparisons with other algorithms, we observed no loss in fidelity despite the several-fold reduction in computational cost associated with the present approach. In particular, conformational down-selection was able to reproduce all TSs of a complex multistep Ireland−Claisen rearrangement that had previously been resolved manually, (re)discover the lowest-barrier stereoisomeric product published to date (out of over 300 possible) for competing DA ring closures of a model ketothioester, and converge the first DFT-level-intended TSs for conformationally complex and competing tetrapeptide cyclization pathways. These demonstrations establish the versatility of using ML classifiers to down-select promising reaction conformers and thus mitigate the additional cost of incorporating conformational sampling into TS localization workflows. Conversely, these benchmarks illustrate the hazards, including overlooked reaction pathways and inaccurate barriers, of neglecting conformational sampling in TS searches. This also comports with the findings of several recent studies across multiple application domains regarding the qualitative importance of conformational sampling for TS searches.[10,24,40−42]

There are still several avenues for improving the current approach. Conformer down-selection reduces costs, but it is still $N_{conf}$ times more costly than a single TS search. One possibility is to use a low-level semiempirical TS search on the down-selected configurations as a preliminary step to further reduce the number of reaction conformers subjected to high-level characterization. Likewise, many reaction conformers end up localizing redundant TSs, which it may be possible to anticipate in advance with a more sophisticated ranking procedure. There are also opportunities for developing an optimal conformer sampling policy. For example, in the third and fourth benchmarks, we deliberately highlighted scenarios where there is asymmetry between reactant-side versus product-side versus TS conformational sampling. We observed scenarios where all were helpful in finding low-lying TSs, but the importance of each is highly contextual, and naive inclusion of all cases can dramatically increase sampling costs. Another avenue for investigation is the degree to which these models could be combined with other common TS algorithms, like NEB,[13] freezing string,[16] and single-ended GSMs.[43] This last represents a particularly interesting case since it should be more robust to reactant conformation.

Among the limitations of the current study are that we have focused exclusively on organic reactions involving neutral species. There are no fundamental obstacles to extending the approach to ionic and organometallic reactions, but data curation and benchmarking need to be performed, which are currently underway. Another limitation is that relatively simple RF models were utilized due to our desire for transferability and the scarcity of intended TS data for training. In the presented benchmarks, these models were able to profitably rank conformers, but they nevertheless still exhibit low confidence in classifying many conformations. As more reaction data become available, we envision more sophisticated models potentially displacing the RF models while keeping the overall workflow relatively unchanged. Similarly, the classification models were only trained to predict the likelihood that a reaction conformation would converge to an intended reaction and did not utilize or consider the reaction activation energy. Future models might also select conformations based on their relative likelihood of yielding a low-barrier TS. Finally, we have focused on conformer selection for double-ended TS searches due to their much lower computational costs. Such down-selection is also compatible with single-ended models, although the featurization presented here would have to be modified.

## ■ ASSOCIATED CONTENT

### Supporting Information

The Supporting Information is available free of charge at https://pubs.acs.org/doi/10.1021/acs.jctc.2c00081.

Additional discussion of feature selection, RF training details, RF performance table, feature importances, supporting results for the DA and peptide benchmarks, summary of reaction types, and description of computational costs. (PDF)

## ■ AUTHOR INFORMATION

### Corresponding Author

**Brett M. Savoie** − *Davidson School of Chemical Engineering, Purdue University, West Lafayette, Indiana 47906, United*



https://doi.org/10.1021/acs.jctc.2c00081
J. Chem. Theory Comput. XXXX, XXX, XXX−XXX

*States;* orcid.org/0000-0002-7039-4039;
Email: bsavoie@purdue.edu

### Authors

**Qiyuan Zhao** − *Davidson School of Chemical Engineering, Purdue University, West Lafayette, Indiana 47906, United States*

**Hsuan-Hao Hsu** − *Davidson School of Chemical Engineering, Purdue University, West Lafayette, Indiana 47906, United States*

Complete contact information is available at: https://pubs.acs.org/10.1021/acs.jctc.2c00081

### Author Contributions

Q.Z. and B.M.S. conceived and designed the study. Q.Z. and H.-H.H. developed the tool, performed the data analysis, and wrote the paper. B.M.S. oversaw the project and wrote the paper.

### Notes

The authors declare no competing financial interest.

Data and Code Availability: The authors declare that the data supporting the findings of this study are available within the paper and its Supporting Information files. The version of YARP and the reaction conformational sampling package used in this study are available through GitHub under the GNU GPL-3.0 License [https://github.com/zhaoqy1996/YARP]. Specifically, the reaction conformational sampling package is stored in [https://github.com/zhaoqy1996/YARP/tree/main/version2.0/CONF_GEN], and the YARP used in this study is in version1.0. Further raw data sources generated by this work are available at https://doi.org/10.6084/m9.figshare.14766624,[33] including raw output files and molecular (reactants, products, and TSs) geometries.

## ■ ACKNOWLEDGMENTS

The work performed by Q.Z., H.-H.H., and B.M.S. was made possible by the Office of Naval Research (ONR) through support provided by the Energetic Materials Program (MURI grant number: N00014-21-1-2476, Program Manager: Dr. Chad Stoltz). B.M.S. also acknowledges partial support for this work from the Dreyfus Program for Machine Learning in the Chemical Sciences and Engineering and the Purdue Process Safety and Assurance Center.

## ■ REFERENCES

(1) Rodrigo, G.; Carrera, J.; Prather, K. J.; Jaramillo, A. DESHARKY: automatic design of metabolic pathways for optimal cell growth. *Bioinformatics* **2008**, *24*, 2554−2556.

(2) Wu, D.; Wang, Q.; Assary, R. S.; Broadbelt, L. J.; Krilov, G. A computational approach to design and evaluate enzymatic reaction pathways: application to 1-butanol production from pyruvate. *J. Chem. Inf. Model.* **2011**, *51*, 1634−1647.

(3) Stine, A.; Zhang, M.; Ro, S.; Clendennen, S.; Shelton, M. C.; Tyo, K. E. J.; Broadbelt, L. J. Exploring De Novo metabolic pathways from pyruvate to propionic acid. *Biotechnol. Prog.* **2016**, *32*, 303−311.

(4) Suleimanov, Y. V.; Green, W. H. Automated discovery of elementary chemical reaction steps using freezing string and Berny optimization methods. *J. Chem. Theory Comput.* **2015**, *11*, 4248−4259.

(5) Zimmerman, P. M. Navigating molecular space for reaction mechanisms: an efficient, automated procedure. *Mol. Simul.* **2015**, *41*, 43−54.

(6) Kim, Y.; Kim, J. W.; Kim, Z.; Kim, W. Y. Efficient prediction of reaction paths through molecular graph and reaction network analysis. *Chem. Sci.* **2018**, *9*, 825−835.

(7) Zhao, Q.; Savoie, B. M. Simultaneously improving reaction coverage and computational cost in automated reaction prediction tasks. *Nat. Comput. Sci.* **2021**, *1*, 479−490.

(8) Young, T. A.; Silcock, J. J.; Sterling, A. J.; Duarte, F. autodE: Automated Calculation of Reaction Energy Profiles—Application to Organic and Organometallic Reactions. *Angew. Chem., Int. Ed.* **2021**, *60*, 4266−4274.

(9) Hirao, H.; Morokuma, K. What is the real nature of ferrous soybean lipoxygenase-1? A new two-conformation model based on combined ONIOM (DFT: MM) and multireference configuration interaction characterization. *J. Phys. Chem. Lett.* **2010**, *1*, 901−906.

(10) Hansen, E.; Rosales, A. R.; Tutkowski, B.; Norrby, P.-O.; Wiest, O. Prediction of Stereochemistry using Q2MM. *Acc. Chem. Res.* **2016**, *49*, 996−1005.

(11) Guan, Y.; Ingman, V. M.; Rooks, B. J.; Wheeler, S. E. AARON: an automated reaction optimizer for new catalysts. *J. Chem. Theory Comput.* **2018**, *14*, 5249−5261.

(12) Henkelman, G.; Jónsson, H. Improved tangent estimate in the nudged elastic band method for finding minimum energy paths and saddle points. *J. Chem. Phys.* **2000**, *113*, 9978−9985.

(13) Henkelman, G.; Uberuaga, B. P.; Jónsson, H. A climbing image nudged elastic band method for finding saddle points and minimum energy paths. *J. Chem. Phys.* **2000**, *113*, 9901−9904.

(14) Peters, B.; Heyden, A.; Bell, A. T.; Chakraborty, A. A growing string method for determining transition states: Comparison to the nudged elastic band and string methods. *J. Chem. Phys.* **2004**, *120*, 7877−7886.

(15) Zimmerman, P. M. Growing string method with interpolation and optimization in internal coordinates: Method and examples. *J. Chem. Phys.* **2013**, *138*, 184102.

(16) Behn, A.; Zimmerman, P. M.; Bell, A. T.; Head-Gordon, M. Efficient exploration of reaction paths via a freezing string method. *J. Chem. Phys.* **2011**, *135*, 224108.

(17) Baker, J.; Kessi, A.; Delley, B. The generation and use of delocalized internal coordinates in geometry optimization. *J. Chem. Phys.* **1996**, *105*, 192−212.

(18) O'Boyle, N. M.; Vandermeersch, T.; Flynn, C. J.; Maguire, A. R.; Hutchison, G. R. Confab-Systematic generation of diverse low-energy conformers. *J. Cheminf.* **2011**, *3*, 8.

(19) Pracht, P.; Bohle, F.; Grimme, S. Automated exploration of the low-energy chemical space with fast quantum chemical methods. *Phys. Chem. Chem. Phys.* **2020**, *22*, 7169−7192.

(20) Zimmerman, P. M. Automated discovery of chemically reasonable elementary reaction steps. *J. Comput. Chem.* **2013**, *34*, 1385−1392.

(21) Grambow, C. A.; Pattanaik, L.; Green, W. H. Deep learning of activation energies. *J. Phys. Chem. Lett.* **2020**, *11*, 2992−2997.

(22) Xie, X.; Clark Spotte-Smith, E. W.; Wen, M.; Patel, H. D.; Blau, S. M.; Persson, K. A. Data-Driven Prediction of Formation Mechanisms of Lithium Ethylene Monocarbonate with an Automated Reaction Network. *J. Am. Chem. Soc.* **2021**, *143*, 13245−13258.

(23) Yang, M.; Zou, J.; Wang, G.; Li, S. Automatic reaction pathway search via combined molecular dynamics and coordinate driving method. *J. Phys. Chem. A* **2017**, *121*, 1351−1361.

(24) Vitek, A. K.; Jugovic, T. M. E.; Zimmerman, P. M. Revealing the strong relationships between ligand conformers and activation barriers: a case study of bisphosphine reductive elimination. *ACS Catal.* **2020**, *10*, 7136−7145.

(25) Breiman, L. Random forests. *Mach. Learn.* **2001**, *45*, 5−32.

(26) Bannwarth, C.; Ehlert, S.; Grimme, S. GFN2-xTB—An accurate and broadly parametrized self-consistent tight-binding quantum chemical method with multipole electrostatics and density-dependent dispersion contributions. *J. Chem. Theory Comput.* **2019**, *15*, 1652−1671.

(27) Melander, M.; Laasonen, K.; Jónsson, H. Removing external degrees of freedom from transition-state search methods using quaternions. *J. Chem. Theory Comput.* **2015**, *11*, 1055−1062.
(28) Zimmerman, P. Reliable transition state searches integrated with the growing string method. *J. Chem. Theory Comput.* **2013**, *9*, 3043−3050.
(29) Frisch, M. J.; Trucks, G. W.; Schlegel, H. B.; Scuseria, G. E.; Robb, M. A.; Cheeseman, J. R.; Scalmani, G.; Barone, V.; Petersson, G. A.; Nakatsuji, H.; Li, X.; Caricato, M.; Marenich, A. V.; Bloino, J.; Janesko, B. G.; Gomperts, R.; Mennucci, B.; Hratchian, H. P.; Ortiz, J. V.; Izmaylov, A. F.; Sonnenberg, J. L.; Williams-Young, D.; Ding, F.; Lipparini, F.; Egidi, F.; Goings, J.; Peng, B.; Petrone, A.; Henderson, T.; Ranasinghe, D.; Zakrzewski, V. G.; Gao, J.; Rega, N.; Zheng, G.; Liang, W.; Hada, M.; Ehara, M.; Toyota, K.; Fukuda, R.; Hasegawa, J.; Ishida, M.; Nakajima, T.; Honda, Y.; Kitao, O.; Nakai, H.; Vreven, T.; Throssell, K.; Montgomery, J. A., Jr.; Peralta, J. E.; Ogliaro, F.; Bearpark, M. J.; Heyd, J. J.; Brothers, E. N.; Kudin, K. N.; Staroverov, V. N.; Keith, T. A.; Kobayashi, R.; Normand, J.; Raghavachari, K.; Rendell, A. P.; Burant, J. C.; Iyengar, S. S.; Tomasi, J.; Cossi, M.; Millam, J. M.; Klene, M.; Adamo, C.; Cammi, R.; Ochterski, J. W.; Martin, R. L.; Morokuma, K.; Farkas, O.; Foresman, J. B.; Fox, D. J. *Gaussian 16*, Revision C.01; Gaussian Inc.: Wallingford CT, 2016.
(30) Aldaz, C.; Kammeraad, J. A.; Zimmerman, P. M. Discovery of conical intersection mediated photochemistry with growing string methods. *Phys. Chem. Chem. Phys.* **2018**, *20*, 27394−27405.
(31) O'Boyle, N. M.; Banck, M.; James, C. A.; Morley, C.; Vandermeersch, T.; Hutchison, G. R. Open Babel: An open chemical toolbox. *J. Cheminf.* **2011**, *3*, 33.
(32) Hjorth Larsen, A.; Jørgen Mortensen, J.; Blomqvist, J.; Castelli, I. E.; Christensen, R.; Dułak, M.; Friis, J.; Groves, M. N.; Hammer, B.; Hargus, C.; Hermes, E. D.; Jennings, P. C.; Bjerre Jensen, P.; Kermode, J.; Kitchin, J. R.; Leonhard Kolsbjerg, E.; Kubal, J.; Kaasbjerg, K.; Lysgaard, S.; Bergmann Maronsson, J.; Maxson, T.; Olsen, T.; Pastewka, L.; Peterson, A.; Rostgaard, C.; Schiøtz, J.; Schütt, O.; Strange, M.; Thygesen, K. S.; Vegge, T.; Vilhelmsen, L.; Walter, M.; Zeng, Z.; Jacobsen, K. W. The atomic simulation environment—a Python library for working with atoms. *J. Phys.: Condens. Matter* **2017**, *29*, 273002.
(33) Zhao, Q.; Savoie, B. YARP Reaction Dataset. 2022, https://doi.org/10.6084/m9.figshare.14766624.
(34) Grambow, C. A.; Jamal, A.; Li, Y.-P.; Green, W. H.; Zádor, J.; Suleimanov, Y. V. Unimolecular reaction pathways of a γ-ketohydroperoxide from combined application of automated reaction discovery methods. *J. Am. Chem. Soc.* **2018**, *140*, 1035−1048.
(35) Lee, C. W.; Taylor, B. L. H.; Petrova, G. P.; Patel, A.; Morokuma, K.; Houk, K. N.; Stoltz, B. M. An Unexpected Ireland−Claisen Rearrangement Cascade During the Synthesis of the Tricyclic Core of Curcusone C: Mechanistic Elucidation by Trial-and-Error and Automatic Artificial Force-Induced Reaction (AFIR) Computations. *J. Am. Chem. Soc.* **2019**, *141*, 6995−7004.
(36) Maeda, S.; Taketsugu, T.; Morokuma, K. Exploring transition state structures for intramolecular pathways by the artificial force induced reaction method. *J. Comput. Chem.* **2014**, *35*, 166−173.
(37) Wong, C. T. T.; Lam, H. Y.; Song, T.; Chen, G.; Li, X. Synthesis of constrained head-to-tail cyclic tetrapeptides by an imine-induced ring-closing/contraction strategy. *Angew. Chem., Int. Ed.* **2013**, *52*, 10212−10215.
(38) Meutermans, W. D. F.; Golding, S. W.; Bourne, G. T.; Miranda, L. P.; Dooley, M. J.; Alewood, P. F.; Smythe, M. L. Synthesis of difficult cyclic peptides by inclusion of a novel photolabile auxiliary in a ring contraction strategy. *J. Am. Chem. Soc.* **1999**, *121*, 9790−9796.
(39) Marenich, A. V.; Cramer, C. J.; Truhlar, D. G. Universal solvation model based on solute electron density and on a continuum model of the solvent defined by the bulk dielectric constant and atomic surface tensions. *J. Phys. Chem. B* **2009**, *113*, 6378−6396.
(40) Simm, G. N.; Reiher, M. Context-driven exploration of complex chemical reaction networks. *J. Chem. Theory Comput.* **2017**, *13*, 6108−6119.
(41) Calixto, A. R.; Ramos, M. J.; Fernandes, P. A. Conformational diversity induces nanosecond-timescale chemical disorder in the HIV-1 protease reaction pathway. *Chem. Sci.* **2019**, *10*, 7212−7221.
(42) Viegas, L. P. Simplified protocol for the calculation of multiconformer transition state theory rate constants applied to tropospheric OH-initiated oxidation reactions. *J. Phys. Chem. A* **2021**, *125*, 4499−4512.
(43) Zimmerman, P. M. Single-ended transition state finding with the growing string method. *J. Comput. Chem.* **2015**, *36*, 601−611.


https://doi.org/10.1021/acs.jctc.2c00081
J. Chem. Theory Comput. XXXX, XXX, XXX−XXX